


## ORIGINAL ARTICLE

# Functional Segregation of the Right Inferior Frontal Gyrus: Evidence From Coactivation-Based Parcellation

Gesa Hartwigsen <sup>1</sup>, Nicole E. Neef<sup>2</sup>, Julia A. Camilleri<sup>3,4</sup>, Daniel S. Margulies<sup>5</sup> and Simon B. Eickhoff<sup>3,4</sup>

<sup>1</sup>Research Group Modulation of Language Networks, Department of Neuropsychology, Max Planck Institute for Human Cognitive and Brain Sciences, Leipzig, Germany, <sup>2</sup>Department of Neuropsychology, Max Planck Institute for Human Cognitive and Brain Sciences, Leipzig, Germany, <sup>3</sup>Institute of Systems Neuroscience, Medical Faculty, Heinrich Heine University Düsseldorf, Düsseldorf, Germany, <sup>4</sup>Institute of Neuroscience and Medicine, Brain & Behavior (INM-7), Research Centre Jülich, Jülich, Germany and <sup>5</sup>Frontlab, Institut du Cerveau et de la Moelle épinière (ICM), UPMC UMRS 1127, Inserm U 1127, CNRS UMR 7225, Paris, France

Address correspondence to Gesa Hartwigsen, Research Group Modulation of Language Networks, Department of Neuropsychology, Max Planck Institute for Human Cognitive and Brain Sciences Leipzig, Stephanstr. 1a, D-04103 Leipzig, Germany. Email: hartwigsen@cbs.mpg.de (Gesa Hartwigsen); Nicole E. Neef, Department of Neuropsychology, Max Planck Institute for Human Cognitive and Brain Sciences Leipzig Stephanstr. 1a, D-04103 Leipzig, Germany. Email: neef@cbs.mpg.de (Nicole E. Neef)  [orcid.org/0000-0002-8084-1330](https://orcid.org/0000-0002-8084-1330),

Gesa Hartwigsen and Nicole E. Neef contributed equally to this work

## Abstract

Previous studies helped unraveling the functional architecture of the human cerebral cortex. However, a comprehensive functional segregation of right lateral prefrontal cortex is missing. Here, we delineated cortical clusters in right area 44 and 45 based on their task-constrained whole-brain activation patterns across neuroimaging experiments obtained from a large database. We identified 5 clusters that differed with respect to their coactivation patterns, which were consistent with resting-state functional connectivity patterns of an independent dataset. Two clusters in the posterior inferior frontal gyrus (IFG) were functionally associated with action inhibition and execution, while two anterior clusters were related to reasoning and social cognitive processes. A fifth cluster was associated with spatial attention. Strikingly, the functional organization of the right IFG can thus be characterized by a posterior-to-anterior axis with action-related functions on the posterior and cognition-related functions on the anterior end. We observed further subdivisions along a dorsal-to-ventral axis in posterior IFG between action execution and inhibition, and in anterior IFG between reasoning and social cognition. The different clusters were integrated in distinct large-scale networks for various cognitive processes. These results provide evidence for a general organization of cognitive processes along axes spanning from more automatic to more complex cognitive processes.

**Key words:** action, functional connectivity, functional decoding, meta-analysis, social cognition

## Introduction

The right inferior frontal gyrus (IFG) has been associated with various cognitive functions, including attention, motor inhibition and imagery, as well as social cognitive processes or speech functions (Corbetta and Shulman 2002; Hamilton and

Grafton 2008; Aron 2011; Lai et al. 2015; Liu et al. 2016; Matchin and Hickok 2016).

Among these functions, several previous studies assigned this region a key role in response inhibition (Aron et al. 2003; Aron and Poldrack 2006; Chambers et al. 2006; Cai et al. 2014;

Cieslik et al. 2015). In particular, the posterior-most part of the right IFG, corresponding to area 44, was associated with response inhibition during motor execution (Aron et al. 2014). Accordingly, these authors argued that this region might be characterized as a “brake” for stopping or pausing responses. Likewise, it was suggested that right area 44 is also engaged in response inhibition during speech processing (Neef et al. 2016). Other neuroimaging studies have reported that both area 44 and area 45/47 are responsive to increased control demands during word comprehension (Lai et al. 2015) and when efficient sentence comprehension requires inhibition and restructuring of information (Matchin and Hickok 2016). In addition to its role in response inhibition and cognitive control, area 44 was further associated with motor imagery (Guillot et al. 2008), working memory control (Marklund and Persson 2012), as well as imitation and action observation (Heiser et al. 2003; Molnar-Szakacs et al. 2005; Caspers et al. 2010).

Two previous meta-analyses demonstrated that higher-level social cognitive processing occurs in the anterior portions of the right IFG (Bzdok et al. 2012; Adolfi et al. 2017). In particular, theory of mind processing, that is, the attribution of cognitive and affective mental states to oneself and others (Baron-Cohen et al. 2001), was associated with right area 45 while empathy processing was located in both right area 45 and 44. Moreover, Adolfi et al. (2017) reported an overlap of social cognitive, emotional, and interoceptive processes (with the latter referring to processes related to the sense of the physiological condition of the body) in right area 45. In line with these observations, face-based mentalizing also necessitates intact right area 45 and 44 function as revealed by a recent direct cortical stimulation study (Yordanova et al. 2017).

Together, the above-cited studies suggest that the right IFG might be divided into different functional clusters that contribute to various cognitive processes. One hypothesis arising from these studies is the existence of a gradient of functional processing, with more automatic action-related cognitive processes

like motor imagery and inhibitory functions being located more posteriorly in right area 44 while more abstract (social-) cognitive functions might be located more anteriorly, that is, in area 45. To test this hypothesis, we conducted a meta-analytic connectivity-based parcellation (Cieslik et al. 2013; Clos et al. 2013; Bzdok et al. 2016) of the right posterior IFG. Here, we first computed whole-brain coactivation patterns (Eickhoff et al. 2010) for each voxel within a region of interest formed by histologically defined right area 44 and 45 (Amunts et al. 1999) across a wide range of neuroimaging studies based on the BrainMap database (Fox et al. 2014). The resulting individual coactivation profiles were then compared between voxels to identify clusters of voxels with similar coactivation patterns (Eickhoff et al. 2016b). A follow-up meta-analytic connectivity modeling analysis on the derived clusters was performed to reveal the overall and specific coactivation networks of these clusters. Finally, functional associations for the derived clusters were inferred from the extensive meta-data in the BrainMap archive (Fox and Lancaster 2002).

In summary, the present study addressed the question whether different clusters within area 44 and 45 of the right IFG can be associated with different cognitive processes. We thus provide the first characterization of subdivisions, specific connectivity profiles, and functions of the right IFG. Our results show that functional processes in the right IFG can be located along at least two principal functional posterior-to-anterior and dorsal-to-ventral axes.

## Materials and Methods

An overview of the workflow for this study is presented in Figure 1. The different steps are briefly summarized in the following sections, for more detailed information, please refer to recent coactivation based parcellation studies (e.g., Ray et al.

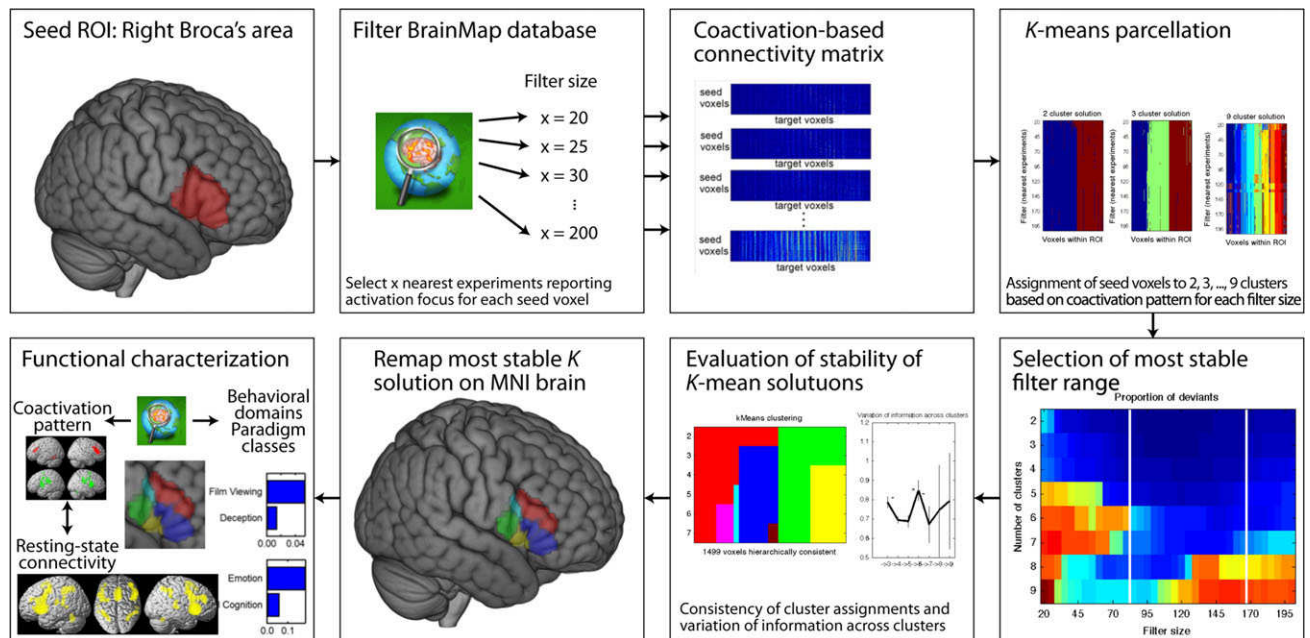


**Figure 1.** Schematic overview of the analyses. For each voxel within the seed region of interest, activation foci from the  $x$  nearest experiments were selected from the BrainMap database. Resulting activation foci were used to generate brain-wide coactivation profiles for each seed voxel and each filter size based on meta-analytic coactivation modeling. Subsequent parcellation of the coactivation matrices was performed with K-means clustering. The optimal range of filter sizes was selected based on the consistency of the cluster assignments. The ensuing evaluation of the K-means solutions was limited to the optimal filter range. The most stable K-means solution was mapped back on the brain and the K clusters were functionally characterized based on their connectivity pattern and BrainMap meta-data.

2015; Muhle-Karbe et al. 2016; Genon et al. 2017) and conceptual overviews (Fox et al. 2014; Eickhoff et al. 2015, 2017).

### Meta-analytic Connectivity Mapping

First, the region of interest (ROI) in the right IFG was defined by using maximum probability maps for area 44 and 45 as provided by the SPM Anatomy Toolbox (Eickhoff et al. 2005, 2006). These maps were derived from quantitative cytoarchitectonic mapping of 10 post-mortem brains (Amunts et al. 1999).

In a second step, the BrainMap database ([www.brainmap.org](http://www.brainmap.org)) (Fox and Lancaster 2002; Laird et al. 2011) was used to compute whole-brain coactivation maps for each voxel within our ROI. Analysis was limited to functional neuroimaging studies in the healthy human brain and did not include interventional studies or group comparisons. The rationale of coactivation analysis is to compute the convergence across those BrainMap experiments where the seed voxel of interest is reported as active (Laird et al. 2013). To characterize task-based functional connectivity, we used a standard pooling procedure across the close spatial neighborhood, with the extent of the spatial filter being systematically varied from including the closest 20–200 experiments in steps of 5 (Chase et al. 2015; Bzdok et al. 2016; Genon et al. 2017). The retrieved experiments were then used to compute the brain-wide coactivation profile of a given seed voxel for each of the 37 filter sizes. We performed a coordinate-based meta-analysis across all foci reported in these experiments to quantify their convergence. The brain-wide coactivation pattern for each individual seed voxel was computed by activation likelihood estimation (ALE) meta-analysis (Turkeltaub et al. 2002; Eickhoff et al. 2009, 2012; Laird et al. 2009) across the experiments that were associated with that particular voxel. The probability distributions of all reported foci were then combined into a modeled activation map for that particular experiment (Turkeltaub et al. 2012). The voxel-wise union of these values (across all experiments associated with a particular seed voxel) yielded an ALE score for each voxel of the brain that describes the coactivation probability with the current seed voxel of each particular location in the brain. Note that this coactivation profile was not thresholded to retain the complete pattern of coactivation likelihood for each voxel (Bzdok et al. 2013b; Cieslik et al. 2013; Bzdok et al. 2016).

### Connectivity-based Parcellation

In the next step, the unthresholded brain-wide coactivation profiles for all seed voxel were combined into an  $N_S \times N_T$  coactivation matrix, where  $N_S$  denotes the number of seed voxels in our ROI (2349 voxels) and  $N_T$  the number of target voxels in the gray matter of the reference brain volume (based on the gray matter probability map, thresholded for the top 10%, at a resolution of  $2 \times 2 \times 2 \text{ mm}^3$ ). The use of 37 different filter sizes resulted in 37 individual coactivation maps, each representing the whole-brain connectivity of the seed voxels at a particular filter size. The parcellation of the VOI was performed with K-means clustering (Hartigan and Wong 1979) implemented in Matlab with  $K = 2, 3, \dots, 9$ , using one minus the correlation between the connectivity patterns of the individual seed voxels as the distance measure. This parcellation was performed for each filter size independently, yielding  $9 \times 37$  independent cluster solutions. K-means clustering aims at minimizing the variance between elements within clusters while maximizing the variance between. For each of the 333 parcellations, we recorded the best solutions from 10 replications (for a similar procedure, see Clos et al. 2013; Bzdok et al. 2015, 2016).

### Selection of Optimal Cluster Solution

The choice of the optimal cluster solution was based on a two-step procedure that includes a first decision on the filter sizes and a second decision on the optimal cluster solution (Clos et al. 2013; Bzdok et al. 2015; Eickhoff et al. 2016a). We first examined the properties of each filter size across all cluster solutions to isolate the most stable range of filter sizes that where then used to select the number of clusters. We selected the filter range with the lowest number of deviants, which minimizes the number of voxels that were assigned differently as compared to the solution from the majority of filters. That is, we identified those filter sizes that reflected solutions most similar to the consensus solution across all filter sizes. Selection was performed based on the weighted sum (across all  $K$ ) of the z-normalized number of deviant voxel assignments at a cut-off at  $Z < -0.5$ , i.e., only those filter sizes where the number of deviants was at least half a standard deviation below the average number of deviants across all filter sizes (85–165 experiments) were included (Fig. 2).

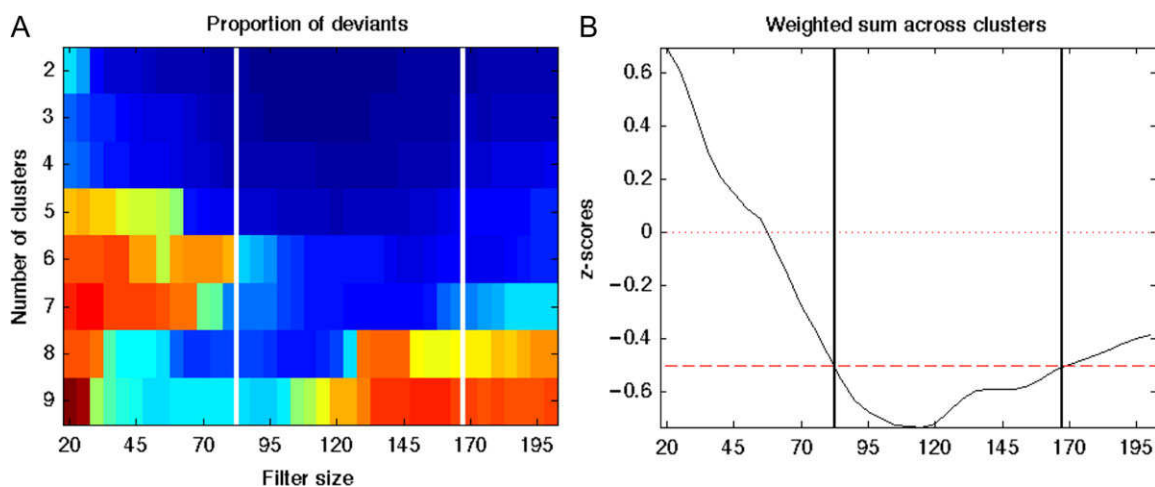


**Figure 2.** Deviants and stability. Z-scores on median-filtered deviants (normalized for  $K$ ). The vertical lines specify the ultimately selected, most stable range of filter size. (A) The proportion of deviants computed across filter size. Warm colors indicate high numbers of deviants and thus less stability; cold colors indicate low numbers of deviants and thus high stability. (B) Maximum z-score of median-filtered deviants.

First, we selected the percentage of voxels that were not related to the dominant parent cluster compared to the  $K - 1$  solution (Fig. 3A). A given  $K$  cluster parcellation was regarded as good solution if the percentage of lost voxels was below the median across all steps and the following clustering step featured a local maximum at the percentage of lost voxels. Secondly, we assessed the number of consistent voxels per cluster, that is, the sizes of the individual cluster after removal of hierarchically inconsistent voxels.  $K$  parcellations were evaluated by considering the proportion of the minimum cluster size to the average cluster size provided by a given  $K$  solution (Fig. 3B). Good solutions were those where the size for the minimum cluster size was more than half of the average cluster size within the  $K$  solution. Thirdly, we assessed the similarity of cluster assignments between the current solution and the neighboring ( $K - 1$  and  $K + 1$ ) solutions by using the variation of information metric (Meila 2007) (Fig. 3C; see Kelly et al. 2010; Kahnt et al. 2012), which assesses the degree of heterogeneity across clusters. Solutions were considered stable if there was a significant increase in the variation of information metric from the current to the subsequent set of solutions (primary criterion) or if there was a significant decrease from the previous to the current clustering step (secondary criterion).

Note that for the subsequent analyses, we only considered hierarchically and spatially consistent voxels located in gray matter.

### Characterization of the Clusters: Task-dependent Connectivity

Functional connectivity profiles of the 5 clusters were characterized with a follow-up meta-analytic connectivity modeling (MACM) analysis that determined the coactivation patterns of the individual clusters. Coactivation patterns for all clusters were obtained by identifying all experiments in the BrainMap database that featured at least one focus of activation in the particular connectivity-based parcellation-derived cluster. Thereafter, an ALE meta-analysis was performed on these experiments. To establish significantly coactivated regions with a given cluster, ALE scores for the MACM analysis of this cluster were compared to a null-distribution reflecting a random spatial association between experiments with a fixed within-experiment distribution of foci (Eickhoff et al. 2009). The observed ALE scores from the meta-analysis of experiments activating within a particular cluster were then tested against ALE scores obtained under a null distribution of random spatial association yielding a  $P$ -value based on the proportion of equal or higher random values (Eickhoff et al. 2012).  $P$ -values were transformed into  $Z$ -scores and thresholded at a cluster-level corrected threshold of  $P < 0.05$  (FWE corrected for multiple comparisons, cf. Eickhoff et al. 2016b). To test for differences in coactivation patterns between pairs of clusters, we performed MACM separately on the experiments associated with either cluster and computed the voxel-wise difference between the ensuing ALE maps (Eickhoff et al. 2011). Finally, specific coactivation patterns for all clusters were computed, indicating brain regions significantly more coactivated with a given cluster than with any of the other clusters.

### Characterization of the Clusters: Task-independent Connectivity

Additionally, specific whole-brain functional connectivity for each cluster was assessed using resting state fMRI as an

independent modality of functional connectivity. These data were obtained from the enhanced NKI/Rockland sample, a part of the International Neuroimaging Datasharing Initiative ([http://fcon\\_1000.projects.nitrc.org/indi/enhanced/index.html](http://fcon_1000.projects.nitrc.org/indi/enhanced/index.html); Nooner et al. 2012). Preprocessing of the data was performed with a standard pipeline in SPM 12 as described elsewhere (Clos et al., 2013; for more details, please also refer to the Supplementary Information: Results section on the additional resting state fMRI-based parcellation analysis). The 5 CBP-derived clusters were used as seeds for the resting state analysis. Linear (Pearson) correlation coefficients between the time series of the seed regions and all other gray matter voxels in the brain were computed to quantify resting state functional connectivity (Circic et al. 2017; Varikuti et al. 2017). Voxel-wise correlation coefficients were transformed into Fisher's  $Z$ -scores and tested for consistency in a flexible factorial model across subjects. The main effect of connectivity for each cluster as well as contrasts between the clusters was tested using standard SPM12 implementations (thresholded at an FWE-corrected cluster level of  $P < 0.05$ ).

### Functional Decoding

Functional characterization of the clusters was based on the meta-data categories "Behavioral Domain and Paradigm Class" in the BrainMap database. The former includes the main categories "action, cognition, emotion, interoception and perception", and related subcategories. Paradigm classes categorize the specific task. Functional profiles for all clusters were determined by using forward and reverse inference as described previously (Clos et al. 2013; Amft et al. 2014; Balsters et al. 2014; Muhle-Karbe et al. 2016). Functional profiles of the clusters were compared at each level of splitting up to the most stable 5-cluster solution. For each comparison of the splitting cluster, the analysis was constrained to all BrainMap experiments activating either cluster.

## Results

### Best Cluster Solution and Stability of the Clustering

$K$ -means clustering was conducted to extract solutions from 2 to 9 clusters. Figure 2A displays the consistency of the cluster assignment for the individual voxels across the 37 filters, indicating the stability of a particular filter size at a given  $K$ -means cluster number. Figure 2B indicates that 85–165 nearest experiments provide the most stable solution for the current analysis. For this reason, the filter size for the nearest "X filter" of the current  $K$ -parcellation was set to the nearest 85–165 experiments.

The 5-cluster solution was identified as the most stable parcellation of our right IFG ROI based on coactivation differences within this region. This solution was supported by the cluster criteria shown in Figure 3. For the criterion "hierarchically inconsistent voxels" (Fig. 3A), the 5 cluster solution featured the maximum in the percentage of lost voxels. The ratio between the "minimum and the average cluster size" was larger than 0.5 for  $K = 2$ ,  $K = 3$ ,  $K = 4$ , and  $K = 5$  (Fig. 3B). The "variation of information between cluster solutions" showed a significant increase between the subsequent ( $K + 1$ ) set of solutions only for the 5 cluster solution (Fig. 3C).

Size and anatomical location of the 5 clusters are summarized in Table 1 and displayed in Figure 4. The clusters are labeled from 1 to 5 according to the hierarchical splitting order (Fig. 4A). At  $K = 2$ , the right IFG was split into an anterior cluster 1 and a posterior cluster 2. At the next level  $K = 3$ , the posterior

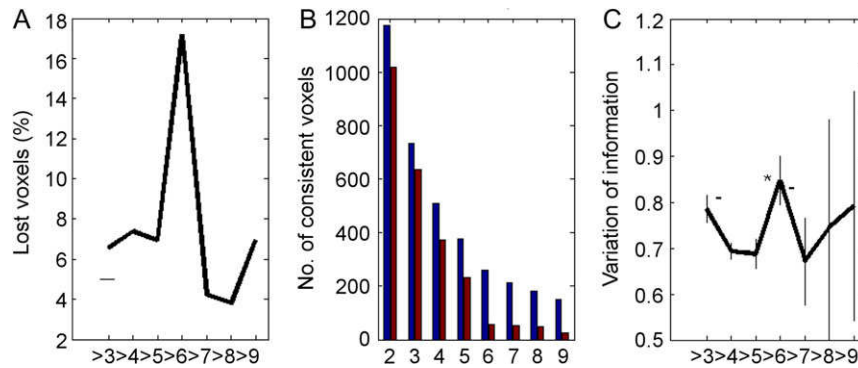


**Figure 3.** Cluster criteria. (A) Percentage of voxels not related to dominant parent cluster compared to the  $K - 1$  solution.  $K = 3$  is considered a good solution (—) because it is located before the maximum and it is lower than the median across all  $K$  solutions;  $K = 5$  is considered a good solution because the following  $K = 6$  features the maximum in the percentage of lost (hierarchically inconsistent) voxels. (B) Mean number of consistent voxel across cluster (blue) and the number of voxels of the smallest individual cluster (red). The ratio between the minimum and the average cluster size was more than 0.5 for  $K = 2$ ,  $K = 3$ ,  $K = 4$ , and  $K = 5$  (good solutions). (C) Variation of information between cluster solutions, significant increase (\*) to the subsequent cluster solution only for  $K = 5$  (primary criterion); significant decrease (–) from previous cluster solution for  $K = 4$  and  $K = 7$  (secondary criterion).

**Table 1** Center-of-gravity for BrainMap coactivation based clustering

Region	Cytoarchitectonic area	x	y	z	Cluster size
Cluster 1	73% 45	52	30	17	625
Cluster 2	46% 44/10% 45	53	15	5	770
Cluster 3	53% 45	54	30	2	573
Cluster 4	24% 45/22% 44	50	19	1	440
Cluster 5	63% 44/16% 45	52	14	19	381

cluster 2 remained the same, and the ventral portion split from the anterior cluster 1. Thus, at  $K = 3$  resulted the final cluster 3 (blue), which was localized at the anterior-ventral part of the IFG (pars triangularis). At  $K = 4$ , the final cluster 4 (yellow) emerged from the ventral portion of the posterior cluster 2 occupying the anterior-ventral part of the IFG pars opercularis extending into the posterior insula. The remaining dorsal portion contained the final cluster 4 (green) at the posterior-ventral part of the IFG pars opercularis. At the last split at  $K = 5$ , the final cluster 5 (cyan) emerged from the posterior parent cluster 1 (emerging at  $K = 3$ ). Cluster 5 was located at the posterior-dorsal part of the IFG pars opercularis merging into the posterior-dorsal part of the IFG pars triangularis in close vicinity of the inferior frontal junction. The final cluster 1 (red) was located in the dorsal part of the pars triangularis of the IFG extending into the inferior frontal sulcus.

### Post-hoc Analysis of Coactivation Patterns of the Clusters

The follow-up MACM analysis on the final cluster solution revealed coactivation maps for each cluster. Specific coactivation based meta-analytic maps are shown in Figure 5A and corresponding peak maxima are reported in Table 2. A cluster-specific connectivity map indicates brain regions that are significantly more coactivated with a given cluster than with any of the other clusters. Common to all coactivation maps is the recruitment of surrounding voxels as well as the involvement of the homotopic area in the left hemisphere. Additionally, cluster 1 showed a specific coactivation with the right paracingulate gyrus, the right superior frontal gyrus (SFG), the left middle frontal gyrus (MFG), and left temporal occipital fusiform gyrus. Cluster 2 showed a specific bilateral coactivation with the anterior cingulate cortex

(ACC), supplementary motor area (SMA), insular cortex, and anterior inferior parietal lobe (IPL), extending into the postcentral gyrus, parietal operculum, opercular cortex, and precentral gyrus. Furthermore, cluster 2 maps showed subcortical regions including the putamen, thalamus and cerebellum. Cluster 3 showed specific coactivation with the left amygdala and bilateral frontal orbital cortex, frontal pole (FP), and the middle temporal gyrus (MTG). Cluster 4 displayed specific coactivation with the left insular cortex, right FP and right temporal pole. Cluster 5 revealed a specific bilateral coactivation with the precentral gyrus, superior parietal lobe (SPL) and the intraparietal sulcus (IPS) extending into the posterior IPL. In addition, cluster 5 maps showed coactivations in the right MTG extending into the right lateral occipital cortex.

Resting state functional connectivity likewise revealed distinct networks associated with each cluster (Fig. 5B). The patterns of functional connectivity, while spatially more diffuse, overlapped with the domain-specific coactivation patterns generated by our MACM analysis. In general, networks were symmetrically distributed across hemispheres and reflect prior divisions of the cerebral cortex into large-scale networks (Yeo et al. 2011). Functional connectivity of cluster 1 overlapped with the fronto-parietal control network (Fig. 6), cluster 2 corresponded partly to the somatomotor and the ventral attention network, cluster 3 overlapped with the default mode network, cluster 4 resembled the ventral attention network, and cluster 5 corresponded to the dorsal attention network.

Additional conjunction analyses across specific coactivation maps and resting state maps for each cluster (Supplementary Table 1) support the main findings and emphasize the stability of our results across independent approaches.

Finally, we calculated an additional MACM analysis for right area 44 only to compare our results with a previous study (Clos et al. 2013) that reported a coactivation-based parcellation of left area 44 only (see Supplementary Results and SI Figs 7–11). While the optimal solution was ambiguous, the 3-cluster solution nicely overlaps with our previous clusters in the posterior part of the larger IFG VOI.

### Post-hoc Functional Characterization: BrainMap Meta-data

In a first step, we determined the quantitative forward and reverse inference on the behavioral domains and paradigm

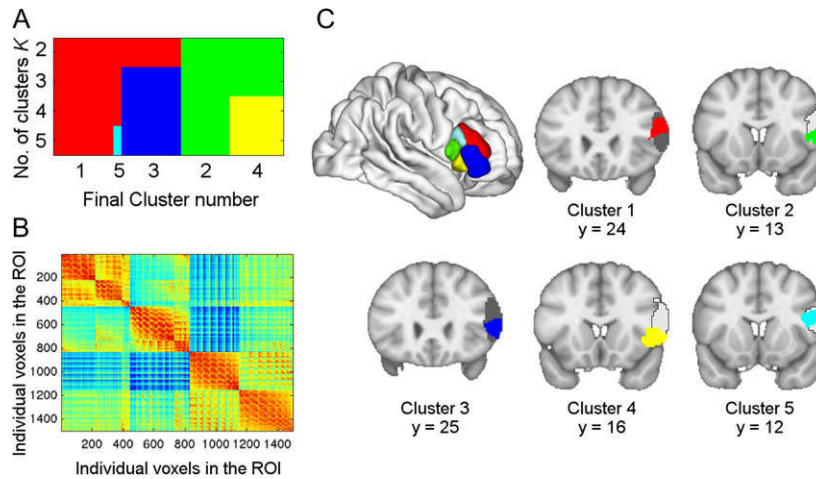


**Figure 4.** Parcellation of right IFG. (A) Pattern of cluster assignment and splitting of clusters across levels of  $K$ . (B) Similarity matrix of the seed voxels reordered according to the splitting scheme derived from  $K$ -means clustering illustrated in (A) above. (C) The 5-cluster solution is rendered on the brain surface. The coronal sections display the location of the clusters on the anatomical template of area 44 (light gray area) and area 45 (dark gray area, Zilles and Amunts 2009).

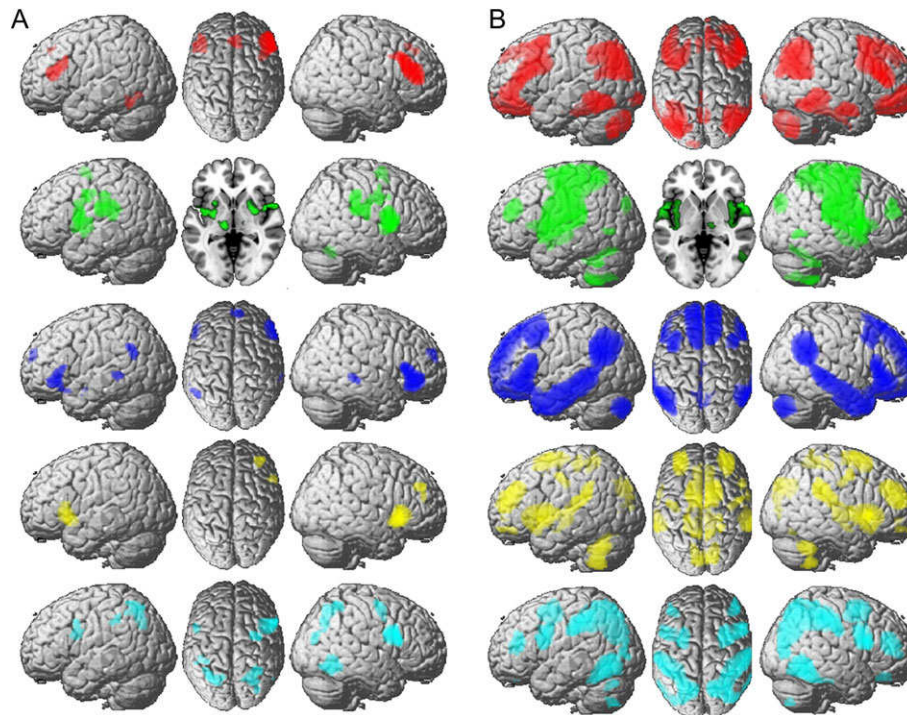


**Figure 5.** Specific connectivity patterns of the 5 clusters. (A) Regions significantly more coactivated with a given cluster than with any of the other 4 clusters. (B) Regions showing significantly more resting state functional connectivity with a given cluster. All results survived a cluster-corrected threshold of  $P < 0.05$ , corrected for multiple comparisons.

classes as sorted in the BrainMap database for each of the 5 clusters separately. Figure 7 displays this assignment of behavioral domains and paradigm classes. Thereby forward inference indicates the probability of activation within a certain cluster given a certain taxonomic label. In other words, activation of a particular cluster is more likely if a certain task was performed. Reverse inference in turn indicates the probability that a particular behavioral domain or paradigm class was present when a given cluster is activated. This inference was constrained by the structure and taxonomic labeling in the BrainMap database.

Inference assigned diverse cognitive domains to the identified clusters, including reasoning, memory, attention, action, and perception (Fig. 7). Specifically, cluster 1 was associated with cognitive reasoning and conflict processing. Cluster 2 was related to action imagination and action execution including speech, music cognition, perception, and deception. Cluster 3 was linked with social cognition and the processing of emotion. Cluster 4 was associated with action inhibition, music cognition, and pain perception. Finally, cluster 5 was associated with memory, encoding, and (spatial) attention.

Table 2 Coactivated regions: specific connectivity

Region	Cytoarchitectonic area	x	y	z	Cluster size
<i>Cluster 1</i>					
R IFG		46	36	6	1349
L IFG		-46	34	16	426
• L middle frontal gyrus		-40	20	32	
R paracingulate gyrus		2	28	46	227
• R superior frontal gyrus		6	38	40	
L temporal occipital fusiform cortex		-42	-52	-18	140
<i>Cluster 2</i>					
L IFG	area 44	-48	4	10	1503
• L IFG	area 44	-58	4	16	
• L IFG	area 44	-62	6	20	
• L putamen		-26	-6	4	
• L insular cortex		-40	-6	0	
• L putamen		-26	8	4	
R STG	TE1.2	56	4	0	1490
• R central opercular cortex		48	4	0	
• R putamen		28	4	2	
• R insular cortex		34	4	12	
L cingulate gyrus, anterior division		-2	4	44	1217
L IPL	PPFpopl	-58	-24	28	1038
• L IPL	PFcm	-42	-34	18	
• L IPL	PF	-60	-28	42	
• L SMG, anterior division	area 2	-52	-28	42	
R IPL	PF	60	-32	24	802
• R IPL	PFop	64	-18	24	
• R IPL	PF	60	-32	40	
• R parietal operculum	OP1	48	-26	24	
• R postcentral gyrus	area 1	60	-14	40	
• R IPL	PFcm	48	-34	34	
R precentral gyrus	area 4p	48	-4	34	209
• R precentral gyrus	area 6	60	6	38	
R cerebellum	VI	22	-58	-26	188
R thalamus	MD	14	-20	6	143
L thalamus	VPM	-14	-18	-2	121
<i>Cluster 3</i>					
R frontal orbital cortex		52	26	-12	852
L frontal orbital cortex		-48	32	-8	416
• L IFG	area 45	-54	22	10	
• L frontal orbital cortex	area 47	-40	16	-18	
R frontal pole		6	58	22	198
L IPL	PGa	-50	-58	28	141
R MTG		64	-34	-2	106
L MTG		-56	-38	0	103
L amygdala		-26	0	-18	87
<i>Cluster 4</i>					
R temporal pole		48	10	-10	1134
L insular cortex		-42	18	-4	643
• L IFG	area 44	-40	20	12	
R frontal pole		38	44	32	167
<i>Cluster 5</i>					
R IFG	area 44	48	14	14	788
R SPL	7A	32	-52	56	667
• R lateral occipital cortex		34	-78	24	
• R SPL	7P	30	-70	42	
L SPL	7A	-34	-62	54	521
• L IPS	hIP3	-24	-64	46	
• L IPS	hIP1	-40	-50	50	
R lateral occipital cortex		52	-64	-12	378
• R inferior temporal gyrus		54	-58	-6	
R middle frontal gyrus		30	-4	56	246
• R precentral gyrus	area 6	42	2	42	

(Continued)

Table 2 (Continued)

Region	Cytoarchitectonic area	x	y	z	Cluster size
L IPS	hIP3	-38	-40	42	108
• L IPS	hIP2	-46	-38	42	
• L IPL	PF	-52	-42	46	
• L IPL	PfT	-46	-32	38	
L IFG	area 44	-52	8	26	92
• L precentral gyrus	area 6	-54	8	38	

Thresholded at  $P < 0.05$ , FWE-corrected for multiple comparisons.

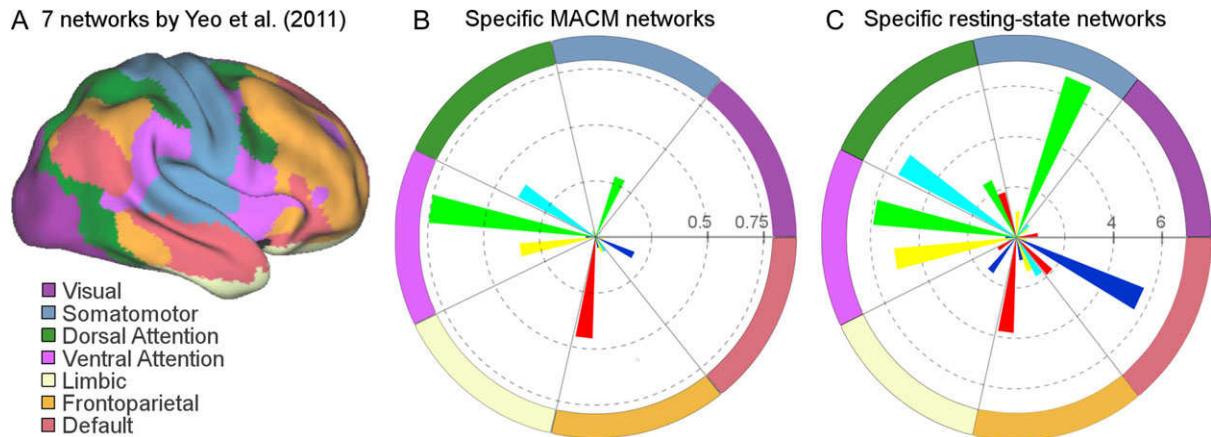


**Figure 6.** Overlap of the right IFG clusters with the widely used seven-network parcellation by Yeo et al. (2011). (A) Seven-network parcellation by Yeo et al. (B) Distribution of the averaged contribution of each of the 5 coactivation maps and (C) of the cluster-specific resting state networks to the 7 modalities. All values are given as Fisher's Z-scores.

To further explore the consistent and distinct functional features of the cluster solution, we examined the features that split at each stage of the clustering hierarchy. Information for contrasting cluster pairs, i.e., where 2 clusters show different behavioral domain and paradigm class information, are shown in Supplementary Figures 1 to 4. At the level of a two-cluster solution (see Supplementary Fig. 1), coactivation maps reflect a fronto-parietal gradient with long-distance coactivations of the anterior IFG with posterior parietal regions also including the MTG and lateral occipital gyrus; and with short-distance coactivations of the posterior IFG with anterior parietal regions also including the postcentral gyrus. The anterior cluster in the right IFG was associated with cognitive functions such as reasoning, memory and conflict processing. In contrast, the posterior cluster of the right IFG was associated with action processing such as action imagination and action execution. At the level of a three-cluster solution (see Supplementary Fig. 2), coactivation of the emerging anterior-dorsal cluster involved parietal, inferior temporal, and lateral occipital regions. Coactivations of the emerging anterior-ventral cluster involved perisylvian parietal in superior temporal regions. Both clusters seem to be involved in social cognitive and emotion processing. Furthermore, the anterior-ventral cluster seems to be additionally recruited during action imagination and the cognition of time. At the level of a four-cluster solution (see Supplementary Fig. 3), coactivation of the emerging posterior-dorsal cluster occurred mainly in the frontal lobes also including the anterior IPS and the posterior IPL (PFm) extending into the posterior division of the STG. In contrast, the emerging posterior-ventral cluster was coactive with regions in close proximity to the central sulcus including large portions of the precentral gyrus in the frontal lobe and

the parietal operculum, the anterior division of the IPL (PFt), and the anterior IPS extending into the SPL and the postcentral gyrus. Both clusters were associated with action processing. Likelihood ratio and probability are higher for the posterior-dorsal cluster to be involved in action execution and action imagination, whereas it is more likely for the posterior-ventral cluster to be involved in the inhibition of an action. Finally, at the level of a 5-cluster solution (see Supplementary Fig. 4), coactivation of the emerging anterior-dorsal cluster is restricted to the frontal lobe, while coactivation of the final cluster 5 involves the precentral gyrus expanding into the MFG, the postcentral gyrus expanding into the SPL and anterior IPS, and the lateral occipital gyrus. It emerged that the final cluster 5 is preferably involved in processes of action execution, spatial attention and imagined movements also involving, for example, mental rotation. In contrast, the final cluster 1 is more likely associated with higher-level executive task processing such as planning and cognitive control.

To further support our main findings, we performed an additional resting state fMRI-based parcellation (see Supplementary Results). In general, these results converge with our main findings, although this analysis favored a 4-cluster solution (see Supplementary Figs 5 and 6). In this analysis, the posterior action-related clusters (i.e., cluster 2 and 4) were merged, which is plausible given the superordinate functional action domain.

## Discussion

This study provides the first coactivation-based parcellation of the right posterior IFG. Our main finding was the segregation of 5 functionally distinct clusters within this region (Fig. 8A). A



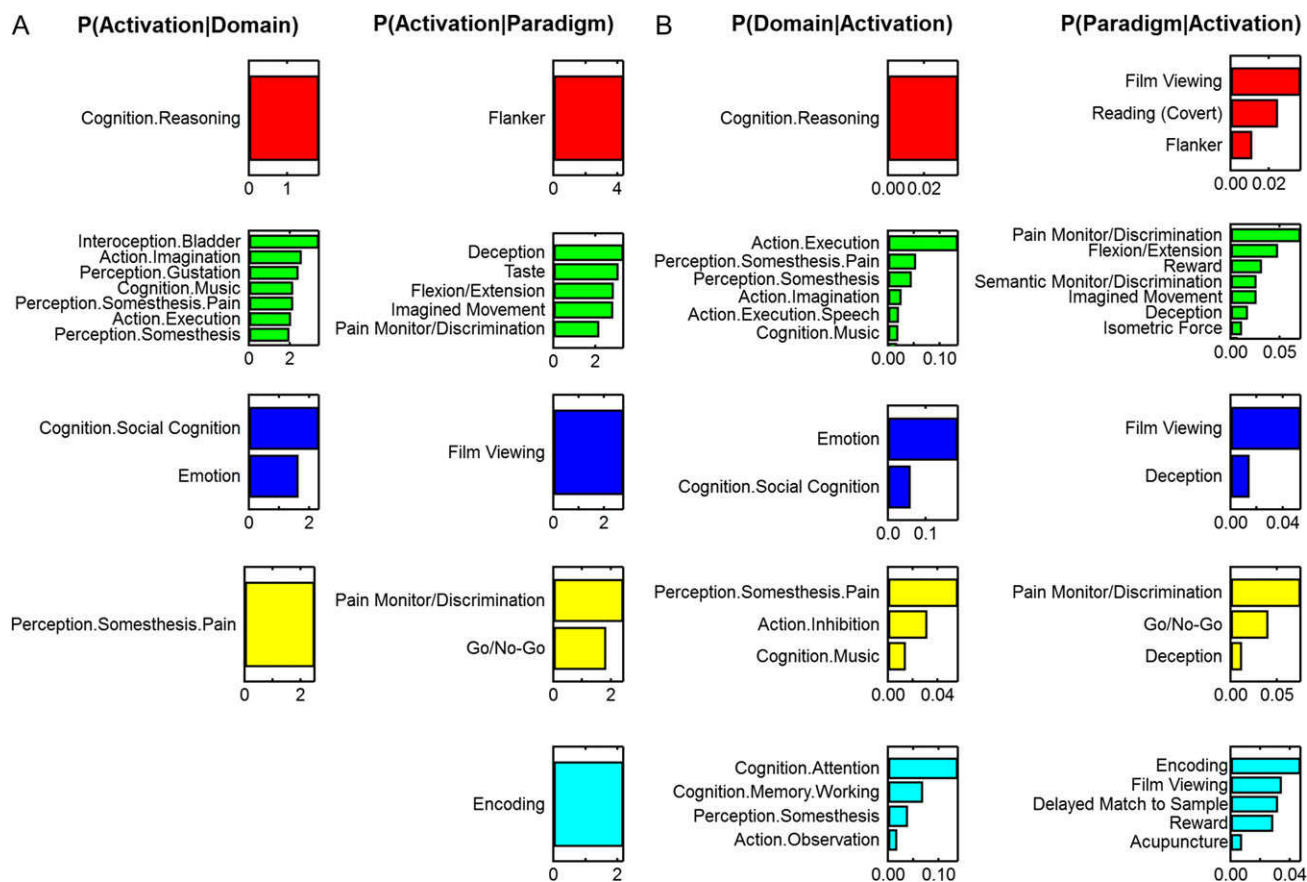


**Figure 7.** Assignment of behavioral domains and paradigm classes to a certain cluster. (A) Forward inference on final clusters: significant activation probability of the cluster given a certain domain (left column) or paradigm (right column). (B) Reverse inference on final clusters: significant probability of domain (left column) or paradigm (right column) occurrence given activation in a cluster. Color code: red = cluster 1, green = cluster 2, blue = cluster 3, yellow = cluster 4, cyan = cluster 5. All functional associations survived a significance threshold of  $P < 0.05$ .

subsequent meta-analytic connectivity modeling of these clusters revealed several principal functional axes. The main axis spanned from motor and perception related functions in posterior portions of the right IFG to more abstract cognitive functions in its anterior part. In addition, two dorsal-to-ventral axes related posterior clusters (cluster 2 and 4) to action inhibition and execution, whereas anterior clusters (cluster 1 and 3) were associated with lower-level mental reasoning and conflict resolution, and with higher-level social cognition and emotion. Finally, we identified a fifth cluster in the most posterior-dorsal part of the IFG that was functionally associated with encoding and spatial attention (Fig. 8B). Notably, none of the here delineated clusters of the right IFG was dedicated to language.

The resulting principal axes exemplify the topography of the macroscale cortical organization (Margulies et al. 2016). For instance, previous studies suggested a posterior-to-anterior gradient for the left prefrontal cortex (Koechlin et al. 2003; Badre 2008; Jeon and Friederici 2013) or the right dorsal premotor cortex (Genon et al. 2017). In the left prefrontal cortex, the functional dissociation is determined by degree of automaticity on the one end and cognitive hierarchy or increasing abstractness on the other end. Highly automatized processes are located in close proximity to the unimodal primary motor areas because they require less heteromodal integration of information. In contrast, increasingly abstract computations that require a stronger amount of cognitive control and transmodal integration are located with increasing distance to primary

areas in anterior portions of the lateral prefrontal cortex (see Jeon and Friederici 2013). Another example is the right dorsal premotor cortex where distinct subregions form a cognitive-motor gradient along a rostro-caudal axis (Genon et al. 2017). We argue that the right IFG can be characterized by a similar organization.

Cytoarchitecturally, the main component of the posterior action-related clusters in our study was area 44, whereas cognition-related clusters were located in area 45 (see Fig. 4C and Table 1). Accordingly, the coactivation based parcellation of the right IFG finds anatomical support for the overarching functional segregation into two domains. Besides cytoarchitecture, receptor architecture enables a more granular parcellation of the inferior frontal gyrus. It was previously demonstrated that left as well as right area 44 could be further segregated into a dorsal and a ventral area, while area 45 was subdivided into an anterior and a posterior cluster (Amunts et al. 2010). Because areas of similar functions show similar receptor patterns (Zilles and Amunts 2009; Amunts et al. 2010; Zilles et al. 2015), the current functional parcellation of the right posterior IFG converges with the anatomical level. Accordingly, the robust functional segregation of subareas across modalities assembles a meaningful regional differentiation (Eickhoff et al. 2017).

We wish to emphasize that while we identified functionally distinct subregions, however, segregated clusters do not process certain functions alone but are implemented in large-scale

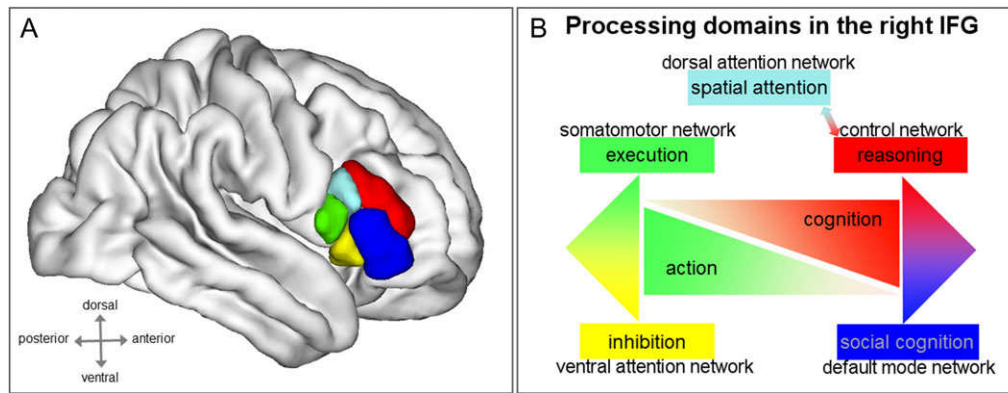


**Figure 8.** Processing domains in the right inferior frontal gyrus. (A) Rendering of the 5 cluster solution on the surface of the right hemisphere. (B) Posterior-to-anterior and dorsal-to-ventral axes of processing domains in the right inferior frontal gyrus.

circuitries. Previous resting state functional connectivity studies have shown that discrete regions of the prefrontal cortex form networks with distributed regions across parietal, temporal, and midline cortex (Yeo et al. 2011). This converges with the notion that despite the existence of functional specializations among areas, functions arise as emergent properties of reciprocally connected brain areas (Mesulam 1981, 1990). More specifically, both task-coactivations and resting state functional connectivity patterns overlapped with modality-specific networks previously described in the neuroimaging literature (i.e., somatomotor network, ventral attention network, dorsal attention network, fronto-parietal control network, and default mode network) (e.g., Yeo et al. 2011). These networks were characterized by distinct topographies with a replication of adjacencies of areas that subserve certain functions along gradients. Such gradients or axes of functional segregation are evident throughout the cerebral cortex and indicate processing streams with input or output systems on one end and the highest level of abstraction on the other end (Margulies et al. 2016).

### Action Processing in the Right Posterior IFG

The two posterior clusters (cluster 2 and cluster 4) were located adjacent to the ventral premotor cortex. Functionally, these two clusters were mainly related to action processing such as action execution, speech execution, action imagination, and action inhibition. Correspondingly, the functional assignment fits well with the earlier mentioned principle of functional organization that is the processing of motor-related or highly automatized cognitive aspects in close proximity to primary and secondary motor areas. A similar topographic organization was observed in a previous coactivation-based parcellation of left area 44 (Clos et al. 2013).

For instance, action imagination such as imagining to move a hand activates the posterior-dorsal part of both the left and the right IFG (Szameitat et al. 2007). Furthermore, predicting the reaching range of a person's foot or hand does likewise involve the right posterior-dorsal IFG (Lamm et al. 2007). Particularly, the integration of the perceptual or emotional domain into motor acts such as visuomotor integration (Macuga and Frey 2011; Papadelis et al. 2016), auditory-motor integration (Tourville et al. 2008; Parkinson et al. 2012; Behroozmand et al. 2016), somatosensory-motor integration (Ehrsson et al. 2000), or the integration of an emotional state in speech production (Pichon and Kell 2013) involve the posterior-dorsal cluster of the right IFG.

Action inhibition has been frequently linked with activity in the right IFG (Aron et al. 2014). Accordingly, our finding that the posterior-ventral cluster 4 was related to inhibitory control converges with multiple quantitative meta-analyses (Cai et al. 2014; Cieslik et al. 2015). However, it is possible to classify 3 subcategories of action inhibition: action cancellation, which is commonly assessed by stop signal tasks, action withholding commonly assessed by Go/NoGo tasks, and inference resolution, which requires the inhibition of competing response programs triggered by Stroop, Simon, Flanker, or antisaccade tasks (Zhang et al. 2017). Specifically the cancellation of an already initiated motor response has been associated with the cluster of the right posterior-ventral IFG as described in cluster 4 (Sebastian et al. 2013; Zhang et al. 2017). Additional support for the assignment of inhibitory control to this cluster comes from a virtual lesion study with transcranial magnetic stimulation. Stimulating the right posterior-ventral IFG impairs stop-signal inhibition under specific attentional demands; the stop signal reaction time is prolonged if and only if a competing flanker stimulus interferes with the stop signal response (Chambers et al. 2007). It appears that the right posterior-ventral IFG is especially relevant for inhibiting already initiated motor response and for inhibitory control during the suppression of competing responses. This implies an involvement of this cluster in the processing of heteromodal aspects during the inhibition of particular motor responses.

Ultimately, heteromodal activity emerges from recurrent interactions within large-scale brain networks. The specific coactivation pattern of the action inhibition cluster involved the right frontal pole, the left IFG and the left insula, a plausible observation that converges with the literature (Swick et al. 2011; Sulpizio et al. 2017). Furthermore, the topography of the resting-state functional connectivity of the action inhibition cluster is reminiscent of the ventral attention network as described by Yeo et al. (2011). Morphological landmarks of the ventral attention network are the inferior frontal gyrus, the frontal pole, the inferior parietal lobe (PFcm), the temporo-occipital part of the middle temporal gyrus, the anterior and posterior division of the cingulate gyrus, and the insular cortex. The ventral attention system is largely lateralized to the right hemisphere and is specialized for the detection of stimuli to direct attention to salient events (Corbetta and Shulman 2002). It is activated when reorienting is unexpected and requires cognitive control (Corbetta and Shulman 2011). Our observation of an overlap between the resting-state network of the right posterior-ventral IFG and the ventral attention network

suggests that a task-related coupling of this control system is likely. Specifically, the involvement of the ventral attention network might help to monitor the switch between perception and action in support of adequate behavior such as the inhibition of a motor response under conditions of heightened response competition.

### Encoding and Spatial Attention Processing in the Right Dorsal IFG

The posterior-dorsal cluster 5 showed specific coactivations in regions previously associated with spatial attention and orienting, including the precentral gyrus, superior parietal lobe (SPL), and the intraparietal sulcus (IPS) extending into the posterior inferior parietal lobe (IPL) (Corbetta 1998; Corbetta and Shulman 2011; de Haan et al. 2015).

Specifically, a region overlapping with our cluster 5 was associated with top-down control during attentional orienting (Yeh et al. 2007; see also Tops and Boksem 2011; Wang et al. 2016). This region has also been proposed to play a role in auditory orienting (Rossi et al. 2014). Moreover, Hampshire et al. (2009) reported increased task-related activity of this IFG cluster in a target detection task under increased attentional load, when targets and distractors were equally frequent. These authors reasoned that the IFG responds to those stimuli of the most relevance to an intended task schema. Another study found increased sensitivity of an IFG cluster that overlapped with our cluster 5 for the processing of novel stimuli that was taken to reflect the evaluation of the potential relevance of incoming sensory stimuli (Downar et al. 2001).

The previously identified role of the right IFG in attention processing converges with the results from our resting-state functional connectivity analysis that revealed a strong overlap with the dorsal attention network (see Yeo et al. 2011), that reflects the coordination of attention to external stimuli (Corbetta and Shulman 2002; Dosenbach et al. 2007).

Aside from the role of cluster 5 in spatial attention, this cluster was also functionally associated with encoding, that is, the memorization of different stimuli. This converges with previous studies that reported increased activity in this cluster of the right IFG during explicit encoding of item-specific letter strings or associative memory formation (Fletcher et al. 1999, 2005; Becker et al. 2017). Congruent with the findings from our specific connectivity analysis, Fletcher et al. (1999) found increased functional connectivity between the right IFG and the right IPL during rule acquisition. Accordingly, Ishai et al. (2002) identified the right IFG as core node for attention, encoding, and visual imagery. These authors reasoned that the right IFG plays a key role for the successful initial encoding of information.

### Social-cognitive and Emotional Processing in the Right Anterior IFG

The two anterior clusters (cluster 1 and 3) showed specific connectivity with regions previously associated with more abstract cognitive functions, including cognitive control and emotional processing. In particular, the dorsal red cluster 1 in area 45 showed specific connectivity with regions that were associated with higher-order executive task processing, planning and monitoring of goal-oriented behavior and higher cognitive operations (e.g., Petrides 2005; Buda et al. 2011; Hart 2016), including the right paracingulate gyrus, right superior and middle frontal gyrus and left temporal occipital fusiform gyrus. Accordingly, functional decoding across forward and reverse

inference associated this region with cognitive reasoning and flanker task processing. Cognitive reasoning subsumes processes related to the mental faculty of forming conclusions, judgments and inferences from facts (see BrainMap database, [www.brainmap.org](http://www.brainmap.org)). The flanker task requires cognitive control, attentional resources, inhibition and response suppression. In particular, this task is assumed to probe interference suppression, that is, the ability to filter out irrelevant information in the environment (Vaidya et al. 2005). A previous study reported increased activity in a right IFG cluster at the border between our clusters 1 and 5 when a colored patch flanked a word target (Morimoto et al. 2008). The upregulation of the right IFG was interpreted as increased cognitive control that served interference suppression. This finding is well in line with our finding that the right anterior IFG was functionally associated with mental reasoning and flanker task processing. This further converges with a recent meta-analysis on interference processing (Xu et al. 2016) that associated a region of the IFG overlapping with our cluster 1 with emotional processing in a face-word conflict task and non-emotional processing when subjects performed a color-word Stroop task. These results show a common neural substrate for emotional and non-emotional interference processing. Together, our findings and other previous results (e.g., Tops and Boksem 2011) provide evidence for a key role of the right anterior IFG in interference resolution, an important cognitive control process (Nee et al. 2007). This notion is further corroborated by the observed resting-state functional connectivity profile for cluster 1 that converges with the previously described fronto-parietal control network (Dosenbach et al. 2007; Yeo et al. 2011), and might be of special relevance for highly adaptive control processes (Cole et al. 2014).

In contrast to cluster 1, the specific connectivity profile for the second anterior cluster 3 in area 45 encompassed regions that were previously associated with emotional processing and higher-level social-cognitive functions, including left amygdala and bilateral frontal orbital cortex, frontal pole and the middle temporal gyrus (Bzdok et al. 2013a; Caruana et al. 2015; Adolfi et al. 2017). In line with the MACM profile for this cluster, functional decoding revealed associations with social cognitive and emotional processes, including film viewing, with the latter triggering core processes of the social cognitive faculty. The assigned role of a subpart of right area 45 in social cognitive and emotional processing fits well with a number of previous studies (Bzdok et al. 2013a; Caruana et al. 2015; Adolfi et al. 2017; Yordanova et al. 2017). For instance, Mossad et al. (2016) reported stronger activation in an IFG region overlapping with our cluster 3 during a false belief task, which converges with a number of previous studies (van Veluw and Chance 2014) and provides further evidence for a contribution of the right IFG to the “mentalizing” network. In particular, the authors suggest that the contribution of the IFG to false belief processing might reflect the inhibition of one’s own belief. The role of this cluster in emotional processing is further supported by the findings of Meder et al. (2016) who reported that outcome valence of a choice task modulated activity in this part of the right IFG. Specifically, the IFG showed stronger activity increases with positive-going prediction errors in a reward-seeking compared to a punishment-avoidance condition, indicating a stronger responsiveness to “better-than-expected” outcomes. The task-independent resting state functional connectivity profile for cluster 3 associated this region with the default mode network (Yeo et al. 2011). It was suggested that the default mode network may set the stage for self-projection and scene construction in the switching between interoceptive and exteroceptive mind states (Buckner and Carroll 2007;

Mars et al. 2013; Li et al. 2015; Bzdok et al. 2016) and strongly overlaps with the previously identified core regions for social cognitive processing, including the prefrontal and parietal cortex (Uddin et al. 2005; Bzdok et al. 2016).

## The Multi-functional Nature of Right and Left Posterior IFG

A previous coactivation-based parcellation study (Clos et al. 2013) characterized the contribution of the left posterior IFG (BA 44) to different cognitive domains. That study reported a 5-cluster solution for right BA 44, with the specific connectivity profiles and associated functions for the different subclusters partly overlapping with and partly diverging from the networks for the posterior part of the right IFG as investigated here.

Our additional MACM analysis for right area 44 only allowed us to compare our results with the previous study (Clos et al. 2013). This additional parcellation revealed inconsistent results with respect to the optimal cluster solution. While the optimal solution was ambiguous, the strong overlap of the 3-cluster solution with our previous clusters in the posterior part of the larger IFG VOI provides further support for our main findings. Specifically, the posterior cluster of our supplementary coactivation-based parcellation (see Supplementary Fig. 8A; green) was associated with action execution and action imagination (Supplementary Fig. 9) and showed a strong overlap with the action execution-related cluster 2 of our main coactivation-based parcellation (Supplementary Fig. 8B; green). The ventral cluster (Supplementary Fig. 8A; blue) was associated with Go/No-Go tasks (Supplementary Fig. 10) and showed a strong overlap with our previously described action inhibition-related posterior-dorsal cluster 4 (Supplementary Fig. 8B; yellow). Finally, the dorsal cluster (Supplementary Fig. 8A; red), which lied adjacent to the posterior inferior frontal sulcus, had an association with cognitive control such as visual attention (Supplementary Fig. 11), and showed a strong overlap with our previously described posterior-dorsal cluster 5 (Supplementary Fig. 8B; light-blue). Altogether, this coactivation-based parcellation of right area 44 only already reflects a posterior-to-anterior gradient with a posterior action and an anterior cognition part.

Most notably, Clos and colleagues (2013) describe a similar functional gradient of left area 44 with a posterior action and an anterior cognition part. This shows that in general both regions are functionally organized alike. However, some functions are shared by both hemispheres, while others are stronger lateralized in either right or left posterior IFG. In particular, we note a congruency of network connectivity and associated function between our posterior action-related clusters and the previous action clusters, that is, cluster 1 for overt speech and cluster 4 for action imagination and rhythmic sequencing in Clos et al. (2013). This points towards a bilateral organization of action processes with a left hemisphere specialization for speech fluency and a right hemisphere specialization for the stopping of motor responses (Neef et al. 2016). The strongest differences between the previous and present study in turn become apparent for language functions. In the previous study, all 5 clusters of left area 44 were associated with various components of language processing, in particular phonological, syntactic, and semantic processing. In contrast, our study converges with other previous results demonstrating that the right posterior IFG harbors a region particularly specialized for spatial attention processes (e.g., Hampshire et al., 2009). With respect to the findings by Clos et al. (2013) in left area 44, it should be noted that we did not find evidence for a 5-cluster solution in right area 44 but for a 3-cluster solution.

## Conclusion

The right inferior frontal gyrus is a heterogeneous area for different processes mainly related to response inhibition and cognitive control. We provide evidence for a segregation of this region into 5 functionally distinct clusters. These regions were distributed among three different principal axes. A first posterior-to-anterior axis located motor functions in the posterior part and more abstract cognitive functions in the anterior IFG. Two dorsal-to-ventral axes provided a more fine-grained description of both faculties, segregating the posterior cluster into a dorsal part for action inhibition and a ventral part for action execution. The anterior IFG was further subdivided into a dorsal cluster for mental reasoning and conflict resolution, and a ventral cluster for higher-level social cognition and emotion. A fifth cluster in the most posterior-dorsal part of the IFG was functionally associated with encoding, spatial navigation and attentional processes.

The different clusters were integrated in distinct large-scale functional networks for various cognitive processes. In summary, our results provide further evidence for a general organization of cognitive processes along large-scale axes in the human cortex spanning from more automatic functions to more complex higher-level cognitive processes.

## Supplementary Material

Supplementary material is available at *Cerebral Cortex* online.

## Funding

This work was supported by the Max Planck Society.

## Notes

*Conflict of Interest:* None declared.

## References

- Adolfi F, Couto B, Richter F, Decety J, Lopez J, Sigman M, Manes F, Ibanez A. 2017. Convergence of interoception, emotion, and social cognition: a twofold fMRI meta-analysis and lesion approach. *Cortex*. 88:124–142.
- Amft M, Bzdok D, Laird AR, Fox PT, Schilbach L, Eickhoff SB. 2014. Definition and characterization of an extended social-affective default network. *Brain Struct Funct*. 220(2):1031–1049.
- Amunts K, Lenzen M, Friederici AD, Schleicher A, Morosan P, Palomero-Gallagher N, Zilles K. 2010. Broca's region: novel organizational principles and multiple receptor mapping. *PLoS Biol*. 8(9):e1000489.
- Amunts K, Schleicher A, Burgel U, Mohlberg H, Uylings HB, Zilles K. 1999. Broca's region revisited: cytoarchitecture and intersubject variability. *J Comp Neurol*. 412:319–341.
- Aron AR. 2011. From reactive to proactive and selective control: developing a richer model for stopping inappropriate responses. *Biol Psychiatry*. 69:e55–e68.
- Aron AR, Fletcher PC, Bullmore ET, Sahakian BJ, Robbins TW. 2003. Stop-signal inhibition disrupted by damage to right inferior frontal gyrus in humans. *Nat Neurosci*. 6:115–116.
- Aron AR, Poldrack RA. 2006. Cortical and subcortical contributions to Stop signal response inhibition: role of the subthalamic nucleus. *J Neurosci*. 26:2424–2433.
- Aron AR, Robbins TW, Poldrack RA. 2014. Inhibition and the right inferior frontal cortex: one decade on. *Trends Cogn Sci*. 18:177–185.

- Badre D. 2008. Cognitive control, hierarchy, and the rostro-caudal organization of the frontal lobes. *Trends Cogn Sci*. 12:193–200.
- Balsters JH, Laird AR, Fox PT, Eickhoff SB. 2014. Bridging the gap between functional and anatomical features of cortico-cerebellar circuits using meta-analytic connectivity modeling. *Hum Brain Mapp*. 35:3152–3169.
- Baron-Cohen S, Wheelwright S, Hill J, Raste Y, Plumb I. 2001. The “Reading the Mind in the Eyes” Test revised version: a study with normal adults, and adults with Asperger syndrome or high-functioning autism. *J Child Psychol Psychiatry*. 42:241–251.
- Becker N, Kalpouzos G, Persson J, Laukka EJ, Brehmer Y. 2017. Differential effects of encoding instructions on brain activity patterns of item and associative memory. *J Cogn Neurosci*. 29:545–559.
- Behroozmand R, Oya H, Nourski KV, Kawasaki H, Larson CR, Brugge JF, Howard MA 3rd, Greenlee JD. 2016. Neural correlates of vocal production and motor control in human Heschl’s Gyrus. *J Neurosci*. 36:2302–2315.
- Buckner RL, Carroll DC. 2007. Self-projection and the brain. *Trends Cogn Sci*. 11:49–57.
- Buda M, Fornito A, Bergstrom ZM, Simons JS. 2011. A specific brain structural basis for individual differences in reality monitoring. *J Neurosci*. 31:14308–14313.
- Bzdok D, Hartwigsen G, Reid A, Laird AR, Fox PT, Eickhoff SB. 2016. Left inferior parietal lobe engagement in social cognition and language. *Neurosci Biobehav Rev*. 68:319–334.
- Bzdok D, Heeger A, Langner R, Laird AR, Fox PT, Palomero-Gallagher N, Vogt BA, Zilles K, Eickhoff SB. 2015. Subspecialization in the human posterior medial cortex. *NeuroImage*. 106:55–71.
- Bzdok D, Laird AR, Zilles K, Fox PT, Eickhoff SB. 2013a. An investigation of the structural, connectional, and functional subspecialization in the human amygdala. *Hum Brain Mapp*. 34:3247–3266.
- Bzdok D, Langner R, Schilbach L, Jakobs O, Roski C, Caspers S, Laird AR, Fox PT, Zilles K, Eickhoff SB. 2013b. Characterization of the temporo-parietal junction by combining data-driven parcellation, complementary connectivity analyses, and functional decoding. *NeuroImage*. 81:381–392.
- Bzdok D, Schilbach L, Vogeley K, Schneider K, Laird AR, Langner R, Eickhoff SB. 2012. Parsing the neural correlates of moral cognition: ALE meta-analysis on morality, theory of mind, and empathy. *Brain Struct Funct*. 217:783–796.
- Cai W, Ryali S, Chen T, Li CS, Menon V. 2014. Dissociable roles of right inferior frontal cortex and anterior insula in inhibitory control: evidence from intrinsic and task-related functional parcellation, connectivity, and response profile analyses across multiple datasets. *J Neurosci*. 34:14652–14667.
- Caruana N, Brock J, Woolgar A. 2015. A frontotemporoparietal network common to initiating and responding to joint attention bids. *NeuroImage*. 108:34–46.
- Caspers S, Zilles K, Laird AR, Eickhoff SB. 2010. ALE meta-analysis of action observation and imitation in the human brain. *NeuroImage*. 50:1148–1167.
- Chambers CD, Bellgrove MA, Gould IC, English T, Garavan H, McNaught E, Kamke M, Mattingley JB. 2007. Dissociable mechanisms of cognitive control in prefrontal and premotor cortex. *J Neurophysiol*. 98:3638–3647.
- Chambers CD, Bellgrove MA, Stokes MG, Henderson TR, Garavan H, Robertson IH, Morris AP, Mattingley JB. 2006. Executive “brake failure” following deactivation of human frontal lobe. *J Cogn Neurosci*. 18:444–455.
- Chase HW, Clos M, Dibble S, Fox P, Grace AA, Phillips ML, Eickhoff SB. 2015. Evidence for an anterior-posterior differentiation in the human hippocampal formation revealed by meta-analytic parcellation of fMRI coordinate maps: focus on the subiculum. *NeuroImage*. 113:44–60.
- Cieslik EC, Mueller VI, Eickhoff CR, Langner R, Eickhoff SB. 2015. Three key regions for supervisory attentional control: evidence from neuroimaging meta-analyses. *Neurosci Biobehav Rev*. 48:22–34.
- Cieslik EC, Zilles K, Caspers S, Roski C, Kellermann TS, Jakobs O, Langner R, Laird AR, Fox PT, Eickhoff SB. 2013. Is there “one” DLPFC in cognitive action control? Evidence for heterogeneity from co-activation-based parcellation. *Cereb Cortex*. 23:2677–2689.
- Ciric R, Wolf DH, Power JD, Roalf DR, Baum GL, Ruparel K, Shinohara RT, Elliott MA, Eickhoff SB, Davatzikos C, et al. 2017. Benchmarking of participant-level confound regression strategies for the control of motion artifact in studies of functional connectivity. *NeuroImage*. 154:174–187.
- Clos M, Amunts K, Laird AR, Fox PT, Eickhoff SB. 2013. Tackling the multifunctional nature of Broca’s region meta-analytically: co-activation-based parcellation of area 44. *NeuroImage*. 83:174–188.
- Cole MW, Repovs G, Anticevic A. 2014. The frontoparietal control system: a central role in mental health. *Neuroscientist*. 20:652–664.
- Corbetta M. 1998. Frontoparietal cortical networks for directing attention and the eye to visual locations: identical, independent, or overlapping neural systems? *Proc Natl Acad Sci USA*. 95:831–838.
- Corbetta M, Shulman GL. 2002. Control of goal-directed and stimulus-driven attention in the brain. *Nat Rev Neurosci*. 3:201–215.
- Corbetta M, Shulman GL. 2011. Spatial neglect and attention networks. *Annu Rev Neurosci*. 34:569–599.
- de Haan B, Bither M, Brauer A, Karnath HO. 2015. Neural correlates of spatial attention and target detection in a multi-target environment. *Cereb Cortex*. 25:2321–2331.
- Dosenbach NU, Fair DA, Miezin FM, Cohen AL, Wenger KK, Dosenbach RA, Fox MD, Snyder AZ, Vincent JL, Raichle ME, et al. 2007. Distinct brain networks for adaptive and stable task control in humans. *Proc Natl Acad Sci USA*. 104:11073–11078.
- Downar J, Crawley AP, Mikulis DJ, Davis KD. 2001. The effect of task relevance on the cortical response to changes in visual and auditory stimuli: an event-related fMRI study. *NeuroImage*. 14:1256–1267.
- Ehrsson HH, Fagergren A, Jonsson T, Westling G, Johansson RS, Forssberg H. 2000. Cortical activity in precision- versus power-grip tasks: an fMRI study. *J Neurophysiol*. 83:528–536.
- Eickhoff SB, Bzdok D, Laird AR, Kurth F, Fox PT. 2012. Activation likelihood estimation meta-analysis revisited. *NeuroImage*. 59:2349–2361.
- Eickhoff SB, Bzdok D, Laird AR, Roski C, Caspers S, Zilles K, Fox PT. 2011. Co-activation patterns distinguish cortical modules, their connectivity and functional differentiation. *NeuroImage*. 57:938–949.
- Eickhoff SB, Constable RT, Yeo BT. 2017. Topographic organization of the cerebral cortex and brain cartography. *NeuroImage*. pii: S1053-8119(17)30122-2. doi: 10.1016/j.neuroimage.2017.02.018
- Eickhoff SB, Heim S, Zilles K, Amunts K. 2006. Testing anatomically specified hypotheses in functional imaging using cytoarchitectonic maps. *NeuroImage*. 32:570–582.

- Eickhoff SB, Jbabdi S, Caspers S, Laird AR, Fox PT, Zilles K, Behrens TE. 2010. Anatomical and functional connectivity of cytoarchitectonic areas within the human parietal operculum. *J Neurosci*. 30:6409–6421.
- Eickhoff SB, Laird AR, Fox PT, Bzdok D, Hensel L. 2016a. Functional segregation of the human dorsomedial prefrontal cortex. *Cereb Cortex*. 26:304–321.
- Eickhoff SB, Laird AR, Grefkes C, Wang LE, Zilles K, Fox PT. 2009. Coordinate-based activation likelihood estimation meta-analysis of neuroimaging data: a random-effects approach based on empirical estimates of spatial uncertainty. *Hum Brain Mapp*. 30:2907–2926.
- Eickhoff SB, Nichols TE, Laird AR, Hoffstaedter F, Amunts K, Fox PT, Bzdok D, Eickhoff CR. 2016b. Behavior, sensitivity, and power of activation likelihood estimation characterized by massive empirical simulation. *NeuroImage*. 137:70–85.
- Eickhoff SB, Stephan KE, Mohlberg H, Grefkes C, Fink GR, Amunts K, Zilles K. 2005. A new SPM toolbox for combining probabilistic cytoarchitectonic maps and functional imaging data. *NeuroImage*. 25:1325–1335.
- Eickhoff SB, Thirion B, Varoquaux G, Bzdok D. 2015. Connectivity-based parcellation: critique and implications. *Hum Brain Mapp*. 36:4771–4792.
- Fletcher P, Buchel C, Josephs O, Friston K, Dolan R. 1999. Learning-related neuronal responses in prefrontal cortex studied with functional neuroimaging. *Cereb Cortex*. 9:168–178.
- Fletcher PC, Zafiris O, Frith CD, Honey RA, Corlett PR, Zilles K, Fink GR. 2005. On the benefits of not trying: brain activity and connectivity reflecting the interactions of explicit and implicit sequence learning. *Cereb Cortex*. 15:1002–1015.
- Fox PT, Lancaster JL. 2002. Opinion: mapping context and content: the BrainMap model. *Nat Rev Neurosci*. 3:319–321.
- Fox PT, Lancaster JL, Laird AR, Eickhoff SB. 2014. Meta-analysis in human neuroimaging: computational modeling of large-scale databases. *Annu Rev Neurosci*. 37:409–434.
- Genon S, Reid A, Li H, Fan L, Müller VI, Cieslik EC, Hoffstaedter F, Langner R, Grefkes C, Laird AR, et al. 2017. The heterogeneity of the left dorsal premotor cortex evidenced by multimodal connectivity-based parcellation and functional characterization. *NeuroImage*. pii: S1053-8119(17)30145-3. doi: 10.1016/j.neuroimage.2017.02.034
- Guillot A, Collet C, Nguyen VA, Malouin F, Richards C, Doyon J. 2008. Functional neuroanatomical networks associated with expertise in motor imagery. *NeuroImage*. 41:1471–1483.
- Hamilton AF, Grafton ST. 2008. Action outcomes are represented in human inferior frontoparietal cortex. *Cereb Cortex*. 18:1160–1168.
- Hampshire A, Thompson R, Duncan J, Owen AM. 2009. Selective tuning of the right inferior frontal gyrus during target detection. *Cogn Affect Behav Neurosci*. 9:103–112.
- Hartigan JA, Wong MA. 1979. A k-means clustering algorithm. *Appl Stat*. 28:100–108.
- Hart J, editor. 2016. *The neurobiology of cognition and behavior*. New York: Oxford University Press.
- Heiser M, Iacoboni M, Maeda F, Marcus J, Mazziotta JC. 2003. The essential role of Broca's area in imitation. *Eur J Neurosci*. 17:1123–1128.
- Ishai A, Haxby JV, Ungerleider LG. 2002. Visual imagery of famous faces: effects of memory and attention revealed by fMRI. *NeuroImage*. 17:1729–1741.
- Jeon HA, Friederici AD. 2013. Two principles of organization in the prefrontal cortex are cognitive hierarchy and degree of automaticity. *Nat Commun*. 4:2041.
- Kahnt T, Chang LJ, Park SQ, Heinzle J, Haynes JD. 2012. Connectivity-based parcellation of the human orbitofrontal cortex. *J Neurosci*. 32:6240–6250.
- Kelly C, Uddin LQ, Shehzad Z, Margulies DS, Castellanos FX, Milham MP, Petrides M. 2010. Broca's region: linking human brain functional connectivity data and non-human primate tracing anatomy studies. *Eur J Neurosci*. 32:383–398.
- Koechlin E, Ody C, Kouneiher F. 2003. The architecture of cognitive control in the human prefrontal cortex. *Science*. 302:1181–1185.
- Lai VT, van Dam W, Conant LL, Binder JR, Desai RH. 2015. Familiarity differentially affects right hemisphere contributions to processing metaphors and literals. *Front Hum Neurosci*. 9:44.
- Laird AR, Eickhoff SB, Fox PM, Uecker AM, Ray KL, Saenz JJ Jr., McKay DR, Bzdok D, Laird RW, Robinson JL, et al. 2011. The BrainMap strategy for standardization, sharing, and meta-analysis of neuroimaging data. *BMC Res Notes*. 4:349.
- Laird AR, Eickhoff SB, Kurth F, Fox PM, Uecker AM, Turner JA, Robinson JL, Lancaster JL, Fox PT. 2009. ALE meta-analysis workflows via the brainmap database: progress towards a probabilistic functional brain atlas. *Front Neuroinform*. 3:23.
- Laird AR, Eickhoff SB, Rottschy C, Bzdok D, Ray KL, Fox PT. 2013. Networks of task co-activations. *NeuroImage*. 80:505–514.
- Lamm C, Fischer MH, Decety J. 2007. Predicting the actions of others taps into one's own somatosensory representations—a functional MRI study. *Neuropsychologia*. 45:2480–2491.
- Li JM, Bentley WJ, Snyder LH. 2015. Functional connectivity arises from a slow rhythmic mechanism. *Proc Natl Acad Sci USA*. 112:E2527–E2535.
- Liu T, Saito H, Oi M. 2016. Obstruction increases activation in the right inferior frontal gyrus. *Soc Neurosci*. 11:344–352.
- Macuga KL, Frey SH. 2011. Selective responses in right inferior frontal and supramarginal gyri differentiate between observed movements of oneself vs. another. *Neuropsychologia*. 49:1202–1207.
- Margulies DS, Ghosh SS, Goulas A, Falkiewicz M, Huntenburg JM, Langs G, Bezgin G, Eickhoff SB, Castellanos FX, Petrides M, et al. 2016. Situating the default-mode network along a principal gradient of macroscale cortical organization. *Proc Natl Acad Sci USA*. 113:12574–12579.
- Marklund P, Persson J. 2012. Context-dependent switching between proactive and reactive working memory control mechanisms in the right inferior frontal gyrus. *NeuroImage*. 63:1552–1560.
- Mars RB, Sallet J, Neubert FX, Rushworth MF. 2013. Connectivity profiles reveal the relationship between brain areas for social cognition in human and monkey temporoparietal cortex. *Proc Natl Acad Sci USA*. 110:10806–10811.
- Matchin W, Hickok G. 2016. 'Syntactic perturbation' during production activates the right IFG, but not Broca's area or the ATL. *Front Psychol*. 7:241.
- Meder D, Madsen KH, Hulme O, Siebner HR. 2016. Chasing probabilities – signaling negative and positive prediction errors across domains. *NeuroImage*. 134:180–191.
- Meila M. 2007. Comparing clusterings—an information based distance. *J Multivar Anal*. 98:873–895.
- Mesulam MM. 1981. A cortical network for directed attention and unilateral neglect. *Ann Neurol*. 10:309–325.
- Mesulam MM. 1990. Large-scale neurocognitive networks and distributed processing for attention, language, and memory. *Ann Neurol*. 28:597–613.

- Molnar-Szakacs I, Iacoboni M, Koski L, Mazziotta JC. 2005. Functional segregation within pars opercularis of the inferior frontal gyrus: evidence from fMRI studies of imitation and action observation. *Cereb Cortex*. 15:986–994.
- Morimoto HM, Hirose S, Chikazoe J, Jimura K, Asari T, Yamashita K, Miyashita Y, Konishi S. 2008. On verbal/non-verbal modality dependence of left and right inferior prefrontal activation during performance of flanker interference task. *J Cogn Neurosci*. 20:2006–2014.
- Mossad SI, AuCoin-Power M, Urbain C, Smith ML, Pang EW, Taylor MJ. 2016. Thinking about the thoughts of others; temporal and spatial neural activation during false belief reasoning. *NeuroImage*. 134:320–327.
- Muhle-Karbe PS, Derrfuss J, Lynn MT, Neubert FX, Fox PT, Brass M, Eickhoff SB. 2016. Co-activation-based parcellation of the lateral prefrontal cortex delineates the inferior frontal junction area. *Cereb Cortex*. 26:2225–2241.
- Nee DE, Wager TD, Jonides J. 2007. Interference resolution: insights from a meta-analysis of neuroimaging tasks. *Cogn Affect Behav Neurosci*. 7:1–17.
- Neef NE, Butfering C, Anwander A, Friederici AD, Paulus W, Sommer M. 2016. Left posterior-dorsal area 44 couples with parietal areas to promote speech fluency, while right area 44 activity promotes the stopping of motor responses. *NeuroImage*. 142:628–644.
- Nooner KB, Colcombe SJ, Tobe RH, Mennes M, Benedict MM, Moreno AL, Panek LJ, Brown S, Zavitz ST, Li Q, et al. 2012. The NKI-Rockland sample: a model for accelerating the pace of discovery science in psychiatry. *Front Neurosci*. 6:152.
- Papadelis C, Arfeller C, Erla S, Nollo G, Cattaneo L, Braun C. 2016. Inferior frontal gyrus links visual and motor cortices during a visuomotor precision grip force task. *Brain Res*. 1650:252–266.
- Parkinson AL, Flagmeier SG, Manes JL, Larson CR, Rogers B, Robin DA. 2012. Understanding the neural mechanisms involved in sensory control of voice production. *NeuroImage*. 61:314–322.
- Petrides M. 2005. Lateral prefrontal cortex: architectonic and functional organization. *Philos Trans R Soc Lond B Biol Sci*. 360:781–795.
- Pichon S, Kell CA. 2013. Affective and sensorimotor components of emotional prosody generation. *J Neurosci*. 33:1640–1650.
- Ray KL, Zald DH, Bludau S, Riedel MC, Bzdok D, Yanes J, Falcone KE, Amunts K, Fox PT, Eickhoff SB, et al. 2015. Co-activation based parcellation of the human frontal pole. *NeuroImage*. 123:200–211.
- Rossi S, Huang S, Furtak SC, Belliveau JW, Ahveninen J. 2014. Functional connectivity of dorsal and ventral frontoparietal seed regions during auditory orienting. *Brain Res*. 1583:159–168.
- Sebastian A, Pohl MF, Kloppel S, Feige B, Lange T, Stahl C, Voss A, Klauer KC, Lieb K, Tuscher O. 2013. Disentangling common and specific neural subprocesses of response inhibition. *NeuroImage*. 64:601–615.
- Sulpizio V, Lucci G, Berchicci M, Galati G, Pitzalis S, Di Russo F. 2017. Hemispheric asymmetries in the transition from action preparation to execution. *NeuroImage*. 148:390–402.
- Swick D, Ashley V, Turken U. 2011. Are the neural correlates of stopping and not going identical? Quantitative meta-analysis of two response inhibition tasks. *NeuroImage*. 56:1655–1665.
- Szameitat AJ, Shen S, Sterr A. 2007. Effector-dependent activity in the left dorsal premotor cortex in motor imagery. *Eur J Neurosci*. 26:3303–3308.
- Tops M, Boksem MA. 2011. A potential role of the inferior frontal gyrus and anterior insula in cognitive control, brain rhythms, and event-related potentials. *Front Psychol*. 2:330.
- Tourville JA, Reilly KJ, Guenther FH. 2008. Neural mechanisms underlying auditory feedback control of speech. *NeuroImage*. 39:1429–1443.
- Turkeltaub PE, Eden GF, Jones KM, Zeffiro TA. 2002. Meta-analysis of the functional neuroanatomy of single-word reading: method and validation. *NeuroImage*. 16:765–780.
- Turkeltaub PE, Eickhoff SB, Laird AR, Fox M, Wiener M, Fox P. 2012. Minimizing within-experiment and within-group effects in Activation Likelihood Estimation meta-analyses. *Hum Brain Mapp*. 33:1–13.
- Uddin LQ, Kaplan JT, Molnar-Szakacs I, Zaidel E, Iacoboni M. 2005. Self-face recognition activates a frontoparietal “mirror” network in the right hemisphere: an event-related fMRI study. *NeuroImage*. 25:926–935.
- Vaidya CJ, Bunge SA, Dudukovic NM, Zalecki CA, Elliott GR, Gabrieli JD. 2005. Altered neural substrates of cognitive control in childhood ADHD: evidence from functional magnetic resonance imaging. *Am J Psychiatry*. 162:1605–1613.
- van Veluw SJ, Chance SA. 2014. Differentiating between self and others: an ALE meta-analysis of fMRI studies of self-recognition and theory of mind. *Brain Imaging Behav*. 8:24–38.
- Varikuti DP, Hoffstaedter F, Genon S, Schwender H, Reid AT, Eickhoff SB. 2017. Resting-state test-retest reliability of a priori defined canonical networks over different preprocessing steps. *Brain Struct Funct*. 222:1447–1468.
- Wang C, Rajagovindan R, Han SM, Ding M. 2016. Top-down control of visual alpha oscillations: sources of control signals and their mechanisms of action. *Front Hum Neurosci*. 10:15.
- Xu M, Xu G, Yang Y. 2016. Neural systems underlying emotional and non-emotional interference processing: an ALE meta-analysis of functional neuroimaging studies. *Front Behav Neurosci*. 10:220.
- Yeh YY, Kuo BC, Liu HL. 2007. The neural correlates of attention orienting in visuospatial working memory for detecting feature and conjunction changes. *Brain Res*. 1130:146–157.
- Yeo BT, Krienen FM, Sepulcre J, Sabuncu MR, Lashkari D, Hollinshead M, Roffman JL, Smoller JW, Zollei L, Polimeni JR, et al. 2011. The organization of the human cerebral cortex estimated by intrinsic functional connectivity. *J Neurophysiol*. 106:1125–1165.
- Yordanova YN, Duffau H, Herbet G. 2017. Neural pathways subserving face-based mentalizing. *Brain Struct Funct*. 222:3087–3105.
- Zhang R, Geng X, Lee TMC. 2017. Large-scale functional neural network correlates of response inhibition: an fMRI meta-analysis. *Brain Struct Funct*. 222:3973–3990.
- Zilles K, Amunts K. 2009. Receptor mapping: architecture of the human cerebral cortex. *Curr Opin Neurol*. 22:331–339.
- Zilles K, Bacha-Trams M, Palomero-Gallagher N, Amunts K, Friederici AD. 2015. Common molecular basis of the sentence comprehension network revealed by neurotransmitter receptor fingerprints. *Cortex*. 63:79–89.